# Small-Signal Stability of Power Systems With Voltage Droop

Jakob Niehues, *Graduate Student Member, IEEE*, Robin Delabays, Anna Büttner, *Member, IEEE*, and Frank Hellmann, *Member, IEEE*

***Abstract*—Guaranteeing the stability of future, inverter-dominated power grids is a central challenge for grid operators, especially when devices from multiple vendors interact. In this work, we derive novel conditions that guarantee small-signal stability. They are independent of device specifics and are locally verifiable in the neighborhood of each bus. The inverters can be highly heterogeneous and implement any control law of frequency, voltage amplitude, active and reactive power, and internal states. The only structural assumptions we make are that the control implements an exact droop relationship between voltage magnitude and reactive power, and that we have a constant $R/X$ ratio throughout the grid. When applied to established models of control designs, we reproduce and generalize established results. To achieve this, we build on the recent small-phase theorem and adapt it to networked systems. The central novelty on the grid modeling side is the use of complex frequency to capture the relevant dynamical behavior of the inverters. While the conditions are sufficient but not necessary, we find that they are not overly conservative in practice. Furthermore, we find that they can identify individual inverters that are the cause of instability.**

***Index Terms*—Grid-forming control, droop control, complex frequency, voltage source converter, small-signal stability.**

## I. Introduction

THE analysis of small-signal stability in multi-machine power grids is a central topic in power grid analysis. The main result of the seminal paper of [1] was to give conditions under which multiple machines and loads, modeled as oscillators, are stable to small perturbations.

Received 17 January 2025; revised 1 July 2025 and 28 August 2025; accepted 14 September 2025. Date of publication 24 September 2025; date of current version 23 February 2026. The work of Jakob Niehues was supported in part by BIMoS (TU Berlin), Studienstiftung des Deutschen Volkes, and in part by the Berlin Mathematical School, funded by the Deutsche Forschungsgemeinschaft (DFG, German Research Foundation) Germany's Excellence Strategy — The Berlin Mathematics Research Center MATH+ under Grant EXC-2046/1, and under Project 390685689. The work of Robin Delabays was supported by the Swiss National Science Foundation under Grant 200021_215336. This work was supported by the OpPoDyn Project, Federal Ministry for Economic Affairs and Climate Action under Grant FKZ:03EI1071A. Paper no. TPWRS-00105-2025. *(Corresponding author: Jakob Niehues.)*

Jakob Niehues is with the Potsdam Institute for Climate Impact Research (PIK), D-14412 Potsdam, Germany, and also with Technische Universität Berlin, 10623 Berlin, Germany (e-mail: jakob.niehues@pikpotsdam.de).

Robin Delabays is with the School of Engineering, University of Applied Sciences of Western Switzerland HES-SO, Sion, Switzerland.

Anna Büttner and Frank Hellmann are with the Potsdam Institute for Climate Impact Research (PIK), D-14412 Potsdam, Germany.

Color versions of one or more figures in this article are available at https://doi.org/10.1109/TPWRS.2025.3613855.

Digital Object Identifier 10.1109/TPWRS.2025.3613855

Since then, a plethora of results from power engineering [2], control theory [3], [4], [5] and theoretical physics [6], [7] have expanded our understanding of the small-signal stability of power systems. However, it remains an active topic of research [8], [9], [10], [11]. In recent years, the topic has gained renewed interest with the introduction of grid-forming converters, which are expected to independently stabilize the synchronous operation of future power grids with high renewable content [12]. Grid-forming control remains an active topic of research, and additionally, often detailed device models are not published by the vendor [13], [14], [15]. There is a wide range of stability results for concrete control strategies, as reviewed in [16]. However, most of them are *ad hoc* and do not generalize naturally to other control schemes.

In this paper, we derive a decentralized stability condition based on the transfer functions that describe how a grid-forming node's frequency and relative voltage velocity react to deviations from power, reactive power, and voltage set points. Remarkably, our results are technology-neutral and apply to all grid-forming nodal actors for which the response to reactive power and voltage set point deviations is proportional, which is an established principle, see for example [17], [18].

The variables used in this work correspond to working with the complex frequency [19] and describing the network state using time-invariant variables that nevertheless fully characterize the operating state at the desired frequency [20], [21]. Such variables are highly effective for identifying grid-forming behavior in the grid [22]. As we will see, an advantage of working in these quantities is that the transfer matrices do not depend on arbitrary quantities such as phase angles. The resulting stability conditions are more explicit, simpler and more easily interpreted than, for example, those of [4], [8], [11]. In particular, the transfer matrices often do not explicitly depend on the operation point around which we linearize, and the conditions can be mapped back to system parameters immediately. We demonstrate this by recovering several classical results as special cases.

As in [8], [11], the central ingredient to our result is the small phase theory introduced in [23]. A companion paper to this work [24] explores the application of this approach to the broad class of adaptive dynamical networks [25], and demonstrates that these methods can match necessary conditions in that setting. This approach can be seen as an extensive generalization of passivity. Passivity-based methods have been previously used to derive decentral stability conditions for scalar networked systems [26] and for power grids [4], [27]. We improve on these

results by giving more broadly applicable conditions that are fully decentralized and less conservative. Similar results were independently obtained in [28], however, only for a heavily restricted class of models when compared to our results.

## II. Statement of the Main Result

We begin by presenting the key assumptions and the main result, using the bare minimum of notation and concepts necessary to state them. For clarity, we first treat lossless systems. The case of homogeneous ratio of resistance to reactance is treated in Section V.

We assume a lossless grid with admittance $\boldsymbol{Y}$. Define $\tilde{\boldsymbol{Y}} := -j\boldsymbol{Y}$, a negative semi-definite Laplace matrix with $\tilde{Y}_{nm} \geq 0$ for all $n \neq m$. Denote nodal complex voltages $\boldsymbol{v} = \boldsymbol{v}_d + j\boldsymbol{v}_q$, a vector with components

$$v_n(t) = V_n(t)e^{j\varphi_n(t)}\,, \tag{1}$$

with phase $\varphi_n$ and amplitude $V_n$. The nodal current injections are $\boldsymbol{\imath} = \boldsymbol{Y}\boldsymbol{v}$, and the nodal power injections $p_n + jq_n = v_n\overline{\imath}_n$.

Quantities at the operating point are written with a superscript $^\circ$. In the co-rotating frame with the grid's nominal frequency, the operating point is given by constant $v_n^\circ$ that induce $V_n^\circ$, $\varphi_n^\circ$, and a power flow solution $p_n^\circ$, $q_n^\circ$ matching the set point.

We assume that the dynamics of the nodes can be formulated in terms of the complex frequency $\eta_n := \dot{v}_n/v_n$ (see [19], [20] for details). Its real part $\varrho_n = \dot{V}_n/V_n$ is the relative amplitude velocity, and its imaginary part, $\omega_n = \dot{\varphi}_n$, is the angular velocity, which is proportional to the frequency. Without loss of generality, we take the complex frequency at the operation point to be equal to zero: $\omega^\circ = \varrho^\circ = 0$. In practical terms, this assumption implies that all nodes have some amount of grid-forming capability.

We can understand the behavior of a broad class of dynamical actors in power grids by considering how their complex frequency reacts to changes in the network state. Near the power flow solution of interest, we can consider the linearized response in terms of the transfer functions. From this perspective, grid-forming actors take the current (or power) as input and supply a voltage as output.

The following analysis focuses on systems that implement a droop relationship between the voltage $V_n$ and the reactive power $q_n$:

$$\hat{q}_n := q_n + \alpha_n V_n, \tag{2}$$

where $\alpha_n \in \mathbb{R}$ denotes the proportionality coefficient. This is the *only* assumption made in the subsequent analysis. Consequently, all models that satisfy this typical condition [18], including those with additional control mechanisms such as $p$–$f$ droop [5], are also encompassed.

For the transfer function representation, we use $p_n$ and the shifted reactive power $\hat{q}_n$ as the nodal inputs, and obtain four transfer functions $T_n^{\bullet\bullet}(s) \in \mathbb{C}$ that describe the nodal behavior near the power flow of interest:

$$\begin{bmatrix}\varrho_n\\ \omega_n\end{bmatrix} = -\begin{bmatrix}T_n^{\varrho\hat{q}} & T_n^{\varrho p}\\ T_n^{\omega\hat{q}} & T_n^{\omega p}\end{bmatrix}\begin{bmatrix}\Delta\hat{q}_n\\ \Delta p_n\end{bmatrix} =: -\boldsymbol{T}_n\begin{bmatrix}\Delta\hat{q}_n\\ \Delta p_n\end{bmatrix}, \tag{3}$$

where all quantities except $\alpha_n$ depend on the Laplace frequency $s$.

Following [20], the matrix elements of $\boldsymbol{T}_n(s)$ are expected to only depend on $p^\circ$, $q^\circ$, and $V^\circ$, but not on the complex voltage $v_n^\circ$ directly. As $v_n^\circ$ is only defined uniquely up to phase, this is a key advantage of working in terms of phase-shift-invariant quantities like $p$, $q$, and $\eta$ rather than, say, $\dot{v}$, $\overline{v}$, and $\imath$, $\overline{\imath}$. This mirrors the choice of power and polar coordinates in [4]. Our main result is:

*Proposition 1 (Small-signal stability of power grids with $V$ and $q$ droop):* Consider a lossless power grid with admittance matrix $\boldsymbol{Y}$ and an operating point with voltage phase angles $\varphi_n^\circ$ and magnitudes $V_n^\circ$, and $\boldsymbol{T}_n(s)$ the transfer function matrices from $\hat{q}_n$, $p_n$, to $\varrho_n$ and $\omega_n$ for some $\alpha_n$.

The operating point is linearly stable if $|\varphi_n^\circ - \varphi_m^\circ| < \pi/2$ for all $n$ and $m$ connected by a line, the $\boldsymbol{T}_n(s)$ are internally stable, and for all $s \in [0, \infty]$ it holds

$$\Re(T_n^{\varrho\hat{q}}) + \Re(T_n^{\omega p}) > 0\,, \tag{4}$$

$$\Re(T_n^{\varrho\hat{q}}) \cdot \Re(T_n^{\omega p}) > \frac{1}{4}\left|T_n^{\varrho p} + \overline{T}_n^{\omega\hat{q}}\right|^2, \tag{5}$$

$$\alpha_n \geq 2\sum_m \tilde{Y}_{nm}\frac{V_m^\circ}{\cos(\varphi_n^\circ - \varphi_m^\circ)}\,. \tag{6}$$

*Proof:* We provide the proof in Appendix D. □

We restrict our analysis to systems for which there is a choice of $\alpha_n$ that eliminates $V_n$ as a nodal state variable by absorbing it into $\hat{q}_n$. Otherwise, the first two conditions might fail for small $s$. The reason for this is that $V_n$ is a local state variable at the bus, while $\dot{V}_n$ is an output. This is in contrast to $\varphi_n$, which does not appear [20]. This mismatch makes the Hermitian part of the transfer function matrix non-definite for small $s$. Choosing $\alpha_n$ such that it eliminates $V_n$ as a nodal state variable makes $\boldsymbol{T}_n$ well-behaved. This can easily be achieved for many models of power grid actors [5], [18] and notably also covers all systems analyzed in [4]. The precise model class is discussed in more detail in Appendix C. From here on, we assume that $\alpha_n$ is chosen in this way. An alternative approach is to restrict the model class such that the transfer function matrix remains well-behaved, e.g., by requiring $T_n^{\varrho p} = T_n^{\omega\hat{q}} = 0$. This alternative approach has been explored independently in depth in [28].

Our conditions align well with established practice in the design of grid-forming power grid actors. The diagonal terms $T_n^{\omega p}$ and $T_n^{\varrho\hat{q}}$ implement a stabilizing reaction of phase and amplitude to active and reactive power deviations, respectively. (4)–(5) together imply that these transfer functions need to have negative real parts and dominate the dynamics. In addition, (5) quantifies how large the crosstalks $T_n^{\omega\hat{q}}$ between reactive power and frequency, and $T_n^{\varrho p}$ between active power and voltage amplitude, may be, without endangering stability.

From the physics of the interconnection, we get a third condition: that the stabilization of the amplitude is sufficiently strong relative to the coupling on the network, as quantified in (6). This condition relates the nodal $V$-$q$ droop ratio $\alpha_n$ to local grid conditions. Note in particular that the lower bound in (6) can be negative, indicating that local grid conditions are so strong that even misconfigured droop relationships can be tolerated.

The remainder of this paper is structured as follows. In Section III, we derive what our main results imply in concrete systems and compare them with the results of [4] and [7]. We then present numerical results for the IEEE 14-bus system in Section IV, which demonstrate that our conditions can be tight in this setting. Finally, we present the generalization to lossy grids in Section V and provide a discussion and outlook in Section VI. The Appendix includes the relevant mathematical definitions, derivations, and proofs.

## III. Concrete Systems

We will now demonstrate that the conditions of Proposition 1 are viable to study the behavior of a wide range of typically considered grid models, and often can even improve on established theoretical considerations. We begin with generalized droop laws.

### A. Generalized Droop

The most general dynamical droop law relating voltage, frequency, active and reactive power is of the form:

$$\dot{\varphi} = c_1\Delta p + c_2\Delta q + c_3\Delta V, \tag{7}$$

$$\dot{V} = c_4\Delta p + c_5\Delta q + c_6\Delta V. \tag{8}$$

Our assumption on exact droop behavior implies $c_6/c_5 = c_3/c_2 =: \alpha$, and we can re-parameterize this as

$$\dot{\varphi} = -C_p^\omega\Delta p - C_q^\omega\Delta\hat{q}, \tag{9}$$

$$\dot{V} = V^\circ\cdot\left(-C_p^V\Delta p - C_q^V\Delta\hat{q}\right), \tag{10}$$

where $\hat{q} := q + \alpha V$. This is also the most general form that the linearized equations of a grid-forming device with $V$ and $q$ droop can take when neglecting internal dynamics [20]. The class of models considered in [5] and [4] Propositions 5 and 6 is a special case of the class studied in this section.

In this section, we discuss and contrast the theoretical results. Below, in Section IV, we will show that our conditions are also remarkably exact in this model class.

The transfer matrix for (9), (10) is

$$\boldsymbol{T}_n(s) = \begin{bmatrix} C_q^V & C_p^V \\ C_q^\omega & C_p^\omega \end{bmatrix}, \tag{11}$$

and (4)–(5) become

$$C_q^V + C_p^\omega > 0 \tag{12}$$

$$C_q^V\cdot C_p^\omega > \frac{1}{4}\left(C_p^V + C_q^\omega\right)^2. \tag{13}$$

The well-established droop principles of controlling $\varphi_n$ with $-\Delta p_n$ and $V_n$ with $-\Delta q_n$ and $-\Delta V_n$ (see for example [17], [18]) are reflected in $T_n^{\omega p} > 0$ and $T_n^{\varrho\hat{q}} > 0$. Equations (12)–(13) tell us that these coefficients need to have the same sign and need to be positive. Equation (13) further quantifies that cross-coupling, reflected by $T_n^{\varrho p}$ and $T_n^{\omega\hat{q}}$, needs to be sufficiently small in comparison.

As long as the established main couplings $C_q^V$, $C_p^\omega$ are positive, there is a band of stable cross-couplings given by

$$C_q^\omega \in -C_p^V + 2\sqrt{C_q^V C_p^\omega}\times(-1,1) \tag{14}$$

and vice versa with $C_q^\omega \leftrightarrow C_p^V$.

The case considered in [4] Proposition 5 corresponds to $C_p^V = C_q^\omega = 0$. Then our stability conditions simplify to $C_q^V > 0$ and $C_p^\omega > 0$ together with the condition on $\alpha$. The conditions presented here improve upon those in Proposition 5 of [4] for this model class. They require that $C_p^\omega$ and $\alpha_n$ are larger than a positive constant that depends on the entire network, and assume the signs of $C_q^V$ and $C_p^\omega$ from the outset. In contrast, we find no bound other than the 'sign' on the $C$, and our lower bound for $\alpha_n$ is a local quantity that can even become negative. We will illustrate that this occurs in practical grid situations in the section on numerical experiments.

### B. Third-Order Models

We now compare our results to established conditions in the widely studied case of second-order phase dynamics and voltage control. For this purpose, we employ a single internal variable $x_n$ that represents the phase velocity (angular frequency) relative to the nominal frequency. For purposes of regularization, we further introduce a first-order feed-through term with coefficient $\delta_n$:

$$\dot{\varphi}_n = x_n - \delta_n\Delta p_n\,, \tag{15}$$

$$\tau_{p_n}\dot{x}_n = -D_n x_n - k_{p_n}\Delta p_n\,, \tag{16}$$

$$\tau_{q_n}\dot{V}_n = -\Delta V_n - k_{q_n}\Delta q_n\,. \tag{17}$$

At $\delta_n = 0$ we have pure second-order phase dynamics. We adapted the notation of the droop-controlled inverter model of [5], which we recover at $\delta_n = 0$. With $k_{q_n} = \alpha_n^{-1}$, the transfer matrix is given by

$$\boldsymbol{T}_n(s) = \begin{bmatrix} (V_n^\circ\alpha_n\tau_{q_n})^{-1} & 0 \\ 0 & \delta_n + \frac{k_{p_n}}{s\tau_{p_n}+D_n} \end{bmatrix}, \tag{18}$$

assuming $\tau_{p_n} > 0$ and $\tau_{q_n} > 0$. A similar model is the third-order model for synchronous machines [18], where the voltage dynamics are slightly different:

$$\tau_{V_n}\dot{V}_n = -\Delta V_n - X_n\Delta(q_n/V_n)\,, \tag{19}$$

with transient reactance $X_n \geq 0$. The transfer matrices of both models are identical via the invertible mapping

$$X_n = V_n^\circ k_{q_n}\left(1 + 2\frac{k_{q_n}q_n^\circ}{V_n^\circ}\right)^{-1}, \tag{20}$$

$$\tau_{V_n} = \tau_{q_n}\left(1 + 2\frac{k_{q_n}q_n^\circ}{V_n^\circ}\right)^{-1}. \tag{21}$$

This transfer matrix also represents the dynamics of virtual synchronous machines [29], quadratic droop control [30], reactive current control [10], and some controls with adaptive inertia [31] through similar mappings.

For the nodal transfer matrices to be stable as required by Proposition 1, we need $D_n > 0$. Conditions (4)–(5) are fulfilled at all $s$ as long as $\delta_n > 0$, $k_{p_n} > -\delta_n D_n$, and $\alpha_n > 0$.

At $\delta_n = 0$ and $s = j\infty$, we have $T_n^{\omega p} = 0$ and violate (5). However, this is sufficient to establish semi-stability at $\delta_n = 0$, because stability holds for arbitrarily small $\delta_n$ and the eigenvalues of the system's Jacobian are continuous functions of the

TABLE I
SIMULATION PARAMETERS

| parameter | $C^V_{q,n}$ | $C^\omega_{p,n}$ | $C^V_{p,n}$ | $C^\omega_{q,n}$ |
|---|---|---|---|---|
| lower | 0.0 | 0.0 | -0.1 | $-C^V_{p,n} - \sqrt{C^V_{q,n} C^\omega_{p,n}}$ |
| upper | 1.0 | 1.0 | 0.1 | $-C^V_{p,n} + \sqrt{C^V_{q,n} C^\omega_{p,n}}$ |

parameters. Furthermore, including gain information allows to treat this system at $\delta_n = 0$, too [24].

In [5], stability conditions for this model were given in terms of matrix inequalities with a similar interpretation to our analysis: the diagonal couplings $T_n^{\varrho\hat{q}}$ and $T_n^{\omega p}$ need to be strong in the positive direction, while the off-diagonal cross-couplings need to be bounded relatively. We obtain a similar result, which, however, is decentralized and thus easier to analyze and implement.

In [5], it was also observed that decreasing $k_{q_n}$ can increase stability by weakening the cross-coupling. This is quantified in our lower bound for $\alpha_n = k_{q_n}^{-1}$ in (6):

$$k_{q_n}^{-1} \geq 2 \sum_m \tilde{Y}_{nm} \frac{V_m^\circ}{\cos(\varphi_n^\circ - \varphi_m^\circ)}. \tag{22}$$

To our knowledge, this lower bound is entirely novel and has not previously been reported in the literature. In [7], [32], under the assumption that all nodes in the system are of the same functional form, a bound for $k_{q_n}$ was also derived. This bound can be tighter or looser than ours, depending on the operating points.

## IV. SIMULATIONS

To test our stability conditions, we simulated the stability of the IEEE 14-bus system equipped with grid-forming inverters following the generalized droop control given in (9)–(10).

First, we tested the condition given in (6). We stressed the grid by simulating imperfect active and reactive power provision to test how the condition performs under realistic settings, such as voltage amplitudes moderately deviating from the nominal values. We varied all $p^\circ$ and $q^\circ$ randomly by up to 10% around the IEEE 14-bus standard values and optimal values, respectively. To obtain heterogeneous parameters, we drew them from random uniform distributions at each node, see Table I. Node Parameters Were Drawn Independently for All Nodes and From Random Uniform Distributions Between "Lower" and "Upper", Such That Conditions (12)–(13) Hold.

We then computed the sufficient bounds for the $\alpha_n$ to be stable, $\alpha_n^{\text{theory}}$, using (6). Setting all inverters to $\alpha_n^{\text{theory}}$, we then systematically varied one inverter setting to find the critical value $\alpha_n^{\text{crit}}$ necessary for stability.

We see in Fig. 1 that the theoretical prediction is almost perfect across all buses. We also observe that $\alpha_n$ can locally be negative. This demonstrates the power of our theoretical analysis to account for local grid conditions in a far more sophisticated manner than previous analyses. In fact, in the system tested, the errors between the predicted and simulated $\alpha_n$ are on the order of machine precision, except when $\alpha_n^{\text{crit}}$ approaches zero.

Fig. 2 illustrates example trajectories for a stable system where all nodes are at the $\alpha_n^{\text{theory}}$, and an unstable system where

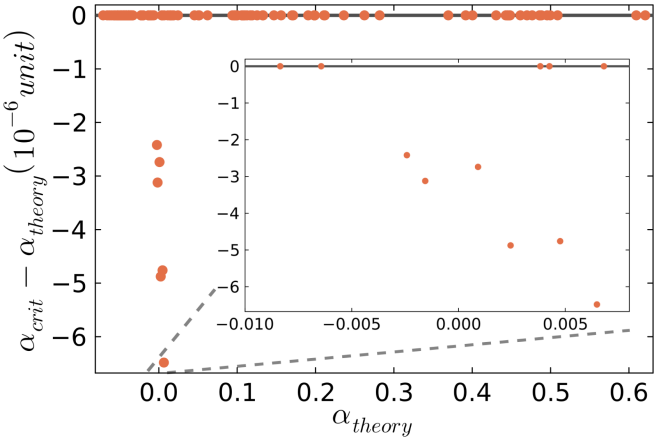


Fig. 1. Numerical small-signal stability of the IEEE 14-bus system. The predicted $\alpha^{\text{theory}}$ closely matches the numerically simulated stability threshold.

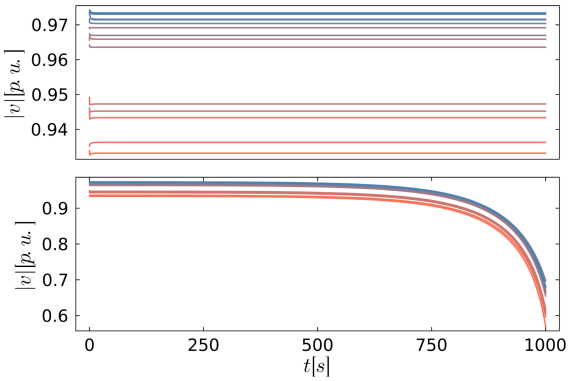


Fig. 2. Trajectories for $\alpha_n = \alpha_n^{\text{theory}}$ (upper) and the case where $\alpha_1 < \alpha_1^{\text{theory}}$. Improperly configured voltage droop at one node causes a slow voltage collapse.

one node (bus 1) violates the theoretical stability guarantee. We observe that the violation leads to a slow voltage collapse within the system. As only one node violates our theoretical bound in this system, our bounds successfully pinpoint the origin of instability in this case.

Finally, we also tested condition (5) for the same setup while keeping the active and reactive power set-points fixed. For the experiment, we set $\alpha_n = \alpha_n^{\text{theory}}$ at each node and varied the strength of the cross-couplings $C_p^V$ and $C_q^\omega$ at individual buses. The results for bus 3 are shown in Fig. 3, all other buses exhibit qualitatively similar behavior.

The stability conditions accurately capture the boundary of stability when the cross-couplings are of comparable magnitude to the main couplings $C_q^V$ and $C_p^\omega$, which is expected for a well-tuned inverter. In the special case $C_p^V = C_q^\omega$, the conditions are almost exact. They become conservative only when the cross-coupling terms differ significantly, which corresponds to an atypical control setting, as such terms are normally designed to be zero or close to zero.

## V. LOSSY LINES

The principles of controlling $V$ with $\hat{q}$ and $\varphi$ with $p$, which are quantified by Proposition 1, are valid for lossless transmission

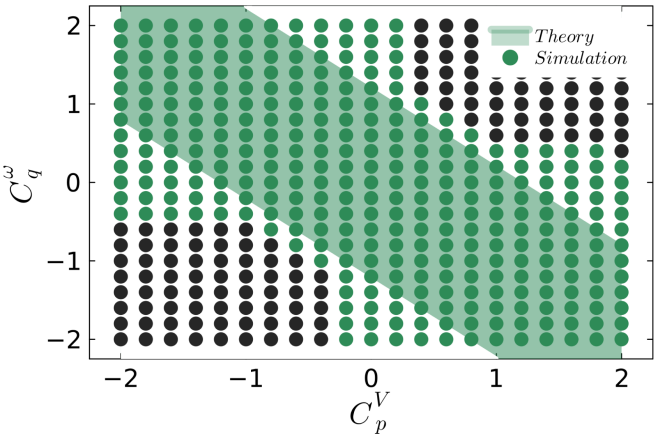


Fig. 3. Numerical small-signal stability of the IEEE 14-bus system in terms of the cross-couplings $C_p^V$, $C_q^\omega$ at node 3. Green and black dots indicate numerical linear stability and instability, respectively, for each parameter configuration. The shaded area indicates our sufficient condition.

lines. In the presence of losses, similar principles hold with $\hat{q}$ and $p$ getting mixed depending on the ratio of resistance $R$ and reactance $X$.

Assuming constant $R/X$ ratio for all lines, we define the angle $\kappa$ through $\tan\kappa := R/X$. We now generalize the rotated admittance matrix by defining $\tilde{\boldsymbol{Y}} := -je^{-j\kappa}\boldsymbol{Y}$, a negative semi-definite Laplace matrix with $\tilde{Y}_{nm} \geq 0$ for all $n \neq m$. The rescaled rotation matrix $\boldsymbol{O}(\kappa)$, and rotated transfer function matrix $\tilde{\boldsymbol{T}}_n$ are defined as

$$\boldsymbol{O}(R/X) := \begin{bmatrix} 1 & -R/X \\ R/X & 1 \end{bmatrix}, \tag{23}$$

$$\boldsymbol{T}_n(s) := \tilde{\boldsymbol{T}}_n(s)\, \boldsymbol{O}(R/X). \tag{24}$$

Note that $\boldsymbol{O}\cos\kappa$ is a rotation matrix. In the lossless case, we have $\boldsymbol{O} = \boldsymbol{I}$, the identity, and $\tilde{\boldsymbol{T}}_n = \boldsymbol{T}_n$. The nodes now obey

$$\begin{bmatrix} \varrho_n \\ \omega_n \end{bmatrix} = -\tilde{\boldsymbol{T}}_n(s) \left( \begin{bmatrix} \Delta q_n \\ \Delta p_n \end{bmatrix} + \boldsymbol{O} \begin{bmatrix} \alpha_n \Delta V_n \\ 0 \end{bmatrix} \right). \tag{25}$$

This way, the conditions of Proposition 1 for $\boldsymbol{T}_n$ and $\alpha_n$ also hold for lossy grids, with an analogous proof, because the admittance can be rotated real for the analysis of the transmission lines' transfer matrix.

What does this parametrization mean in practice? To interpret the conditions on $\boldsymbol{T}_n$, consider that it can be seen as a transfer matrix from the lines' output

$$\boldsymbol{O}^{-1} \begin{bmatrix} \Delta q_n \\ \Delta p_n \end{bmatrix} + \begin{bmatrix} \alpha_n \Delta V_n \\ 0 \end{bmatrix} \tag{26}$$

to $[\rho_n \quad \omega_n]^\intercal$. This is a droop between $\hat{q} = q + \alpha V$ as before, and $\hat{p} = p + \alpha V R/X$ instead of just $p$, i.e., the control is adapted to the $R/X$ ratio. This mirrors the control design where current and power are also rotated by the angle defined by $R/X$ [27].

## VI. Discussion and Conclusion

In this paper, we derived fully decentralized small-signal stability conditions for power grids under the assumption of $V$ and $q$ droop, as well as a homogeneous $R/X$ ratio for the lines. The preceding results provide a simple characterization of small-signal stability of heterogeneous grids in terms of transfer matrices between power mismatch on the input side, and frequency and voltage velocity on the output side. Such transfer function-based specifications are natural for the design and specification of decentralized power grid control strategies, and could potentially be directly encoded in grid codes [33]. This is especially interesting as the transfer functions we are concerned with can be measured experimentally [22].

The type of conditions derived here are robust in the sense that, if the numerical range of a nodal transfer matrix is bounded away from zero for all $s$ on the contour (see proof), a perturbation of the transfer matrix of $H_\infty$ norm smaller than the bound can not make the system unstable. However, as we have to assume an exact droop relationship, this robustness does not yet easily extend to actual system parameters.

We expect that our results can be adapted to load models, as the complex frequency approach [19] can also capture load models and grid-following control [34]. A starting point for an extension to line dynamics is given in [28]. An alternative approach is to absorb the line dynamics into the node dynamics in the case of a homogeneous $R/X$, as they are essentially a low-pass filter on the nodal power flow, see Appendix B of [21].

The most significant challenge for our approach is to accurately account for non-droop-like reactions to voltage amplitude deviations. This also prevents us from directly applying the theory to conventional models in the presence of losses. Naively adding in additional voltage dynamics on the nodal side fails due to the sectoriality constraints. Similarly, models that do not have a pass-through like $\delta_n$ in (15) fail our conditions at infinite imaginary $s$.

Lastly, dVOC [35], [36] is covered by our theorem only in the unloaded case. To address these limitations, it will be necessary to accurately incorporate gain information into the stability analysis. The companion paper [24] explores this in the context of adaptive dynamical networks. We leave this extension of the methods introduced in this paper to future work.

## Conflict of Interest

None of the authors have a conflict of interest to disclose.

## Data Availability

Both, the data that supports the findings of this study and the source code used to produce the results are openly available on Zenodo [40].

## Appendix A
## Notational Preliminaries

To prove the above result, we begin by expanding on the notation used above. We want to consider the small-signal stability of power grids with a heterogeneous mix of grid-forming actors. The $N$ nodes are indexed $n$ and $m$, $1 \leq n, m \leq N$. The $E$ edges in the set of edges $\mathcal{E}$ are indexed by ordered pairs $e = (n, m)$,

$n < m$. For any nodal quantity $x_n$, we denote the overall $N$-dimensional vector by $\boldsymbol{x}$. We write $[\boldsymbol{x}]$ for the diagonal matrix with $x_n$ on the diagonal: $[\boldsymbol{x}]_{nm} = \delta_{nm} x_n$, where $\delta_{nm} = 1$ if $n = m$, and 0 else. In general, matrices are uppercase bold, e.g., $\boldsymbol{A}$, and vectors are lowercase bold. We denote with $\mathbf{1}$ the constant vector $1_n = 1$, so the identity matrix is $[\mathbf{1}] = \boldsymbol{I}$, and similarly for $\mathbf{0}$ and $[\mathbf{0}]$.

We denote the imaginary unit $j$, the complex conjugate of a quantity $z$ by $\overline{z}$, the transpose of a vector or matrix $\boldsymbol{A}$ as $\boldsymbol{A}^\intercal$, and the complex transpose by $\boldsymbol{A}^\dagger$.

We will often have two quantities per node, e.g., $z_n$ and $\overline{z}_n$. Stacking the vector of nodal quantities is written as

$$\begin{bmatrix} \boldsymbol{z} \\ \overline{\boldsymbol{z}} \end{bmatrix} . \tag{27}$$

We will also often be looking only at the components associated with a single node $n$ in such a stacked vector. To this end, we introduce the matrix $\boldsymbol{P}_n$ which selects these entries

$$\begin{bmatrix} z_n \\ \overline{z}_n \end{bmatrix} = \boldsymbol{P}_n \begin{bmatrix} \boldsymbol{z} \\ \overline{\boldsymbol{z}} \end{bmatrix} , \tag{28}$$

and its transpose $\boldsymbol{P}_n^\dagger$. Note that $\boldsymbol{P}_n$ are isometries, and $\boldsymbol{P}_n^\dagger \boldsymbol{P}_n$ is an orthogonal projection matrix.

Given a set of nodewise matrices $\boldsymbol{A}_n$, the matrix built from them with the direct sum $\bigoplus$ then acts on our stacked vector as:

$$\bigoplus_n \boldsymbol{A}_n \begin{bmatrix} \boldsymbol{z} \\ \overline{\boldsymbol{z}} \end{bmatrix} := \sum_n \boldsymbol{P}_n^\dagger \boldsymbol{A}_n \boldsymbol{P}_n \begin{bmatrix} \boldsymbol{z} \\ \overline{\boldsymbol{z}} \end{bmatrix} , \tag{29}$$

While the matrix representation of $\bigoplus_n \boldsymbol{A}_n$ is not block diagonal on the stacking $[\boldsymbol{z} \;\; \overline{\boldsymbol{z}}]^\intercal$, it is block diagonal when stacking $[z_1 \;\; \overline{z}_1 \;\; z_2 \;\; \overline{z}_2 \;\; \dots z_n \;\; \overline{z}_n]^\intercal$.

We also introduce the matrix $\boldsymbol{P}_e$ that selects the states related to the edge $e$ from our stacked vector:

$$\boldsymbol{P}_e \begin{bmatrix} \boldsymbol{z} \\ \overline{\boldsymbol{z}} \end{bmatrix} = \boldsymbol{P}_{(n,m)} \begin{bmatrix} \boldsymbol{z} \\ \overline{\boldsymbol{z}} \end{bmatrix} = \begin{bmatrix} z_n \\ \overline{z}_n \\ z_m \\ \overline{z}_m \end{bmatrix} . \tag{30}$$

The $\boldsymbol{P}_e$ are isometries, but $\boldsymbol{P}_e^\dagger \boldsymbol{P}_e$ are not mutually orthogonal. Therefore, a matrix built from $4 \times 4$ matrices $\boldsymbol{A}_e$ as

$$\sum_e \boldsymbol{P}_e^\dagger \boldsymbol{A}_e \boldsymbol{P}_e , \tag{31}$$

is not block diagonal. However, it can be written as the projection of a block diagonal matrix $\bigoplus_e \boldsymbol{A}_e$ and we write:

$$\sum_e \boldsymbol{P}_e^\dagger \boldsymbol{A}_e \boldsymbol{P}_e = \boldsymbol{B}_+^\dagger \bigoplus_e \boldsymbol{A}_e \boldsymbol{B}_+ , \tag{32}$$

for an according $4E \times 2N$ matrix $\boldsymbol{B}_+$ that fulfills this equation.

## Appendix B
## Phase Stability Preliminaries

Our results are based on the Generalized Small Phase Theorem of Chen *et al.* [23]. We prove a straightforward proposition stating that if the transfer matrices of the system under consideration have a block structure, the global stability conditions can be decomposed into local conditions. An immediate application are networked systems that consist of node and edge variables that are coupled according to a graph.

Using this proposition, we give a precise statement of the stability conditions for a power grid of general grid-forming grid actors with $V$ and $q$ droop as introduced above.

For completeness, we begin by recalling the Small Phase Theorem of [23], which provides conditions for the stability of the connected system $\boldsymbol{G}\#\boldsymbol{H}$, in terms of the *numerical range* $W$ and the *angular field of values* $W'$ [37, Sec. 1.0, Def. 1.1.2], [38], [39], defined for a matrix $\boldsymbol{M} \in \mathbb{C}^{N\times N}$ as

$$W(\boldsymbol{M}) = \left\{ \boldsymbol{z}^\dagger \boldsymbol{M} \boldsymbol{z} \,|\, \boldsymbol{z} \in \mathbb{C}^N , \, \boldsymbol{z}^\dagger \boldsymbol{z} = 1 \right\} , \tag{33}$$

$$W'(\boldsymbol{M}) = \left\{ \boldsymbol{z}^\dagger \boldsymbol{M} \boldsymbol{z} \,|\, \boldsymbol{z} \in \mathbb{C}^N , \, \boldsymbol{z}^\dagger \boldsymbol{z} > 0 \right\} . \tag{34}$$

When the numerical range lies in a half complex plane, we introduce the notion of *sectoriality*. Assume that 0 is not in the interior of $W(\boldsymbol{M})$. Define $\overline{\phi}(\boldsymbol{M})$ and $\underline{\phi}(\boldsymbol{M})$ as the maximum and minimum arguments of the elements of such a $W(\boldsymbol{M})$, and $\delta(\boldsymbol{M}) := \overline{\phi}(\boldsymbol{M}) - \underline{\phi}(\boldsymbol{M})$. Then the matrix $\boldsymbol{M}$ is

- *semi-sectorial* if $\delta(\boldsymbol{M}) \leq \pi$;
- *quasi-sectorial* if $\delta(\boldsymbol{M}) < \pi$;
- *sectorial* if $0 \notin W(M)$.

Notice that a non-sectorial matrix $\boldsymbol{M}$ is semi-sectorial if 0 is on the boundary of $W(\boldsymbol{M})$.

Let $\mathcal{R}H_\infty^{m\times m}$ denote the set of $m \times m$ transfer matrices of real-rational proper stable systems. For these systems, all the poles of any $\boldsymbol{H}(s) \in \mathcal{RH}_\infty^{m\times m}$ (should there be any) are in the open left-hand side of the plane. A system $\boldsymbol{G} \in \mathcal{R}H_\infty^{m\times m}$ is called frequency-wise sectorial if $\boldsymbol{G}(s)$ is sectorial for all $s \in j\mathbb{R}$. A system $\boldsymbol{G}(s)$ is semi-stable if its poles are in the closed left half plane. Take $j\Omega$ the set of poles on the imaginary axis, and $j\mathbb{R} \setminus j\Omega$ the indented imaginary axis with half-circles of radius $\epsilon \in \mathbb{R}$ around the poles and of radius $1/\epsilon$ around $\infty$ if it is a zero. These $\epsilon$-detours lie in the right half-plane. We call this indented imaginary axis "the contour". A system is semi-stable frequency-wise semi-sectorial if $\boldsymbol{G}(s)$ has constant rank along the contour and is semi-sectorial on $j\mathbb{R} \setminus j\Omega$.

The phase center is defined as $\gamma[\boldsymbol{G}(s)] := \{\overline{\phi}[\boldsymbol{G}(s)] + \underline{\phi}[\boldsymbol{G}(s)]\}/2$, and without loss of generality, we assume that $\gamma[\boldsymbol{G}(\epsilon^+)] := \lim_{\epsilon \searrow 0} \gamma[\boldsymbol{G}(\epsilon)] = 0$.

We can now recall Chen *et al.*'s Small Phase Theorem.

*Theorem 2 (Generalized Small Phase Theorem, [23]):* Let $\boldsymbol{G}$ be semi-stable frequency-wise semi-sectorial with $j\Omega$ being the set of poles on the imaginary axis, and $\boldsymbol{H} \in \mathcal{R}H_\infty$ be frequency-wise sectorial. Then $\boldsymbol{G}\#\boldsymbol{H}$ is stable if

$$\sup_{s \in j[0,\infty]\setminus j\Omega} \left[ \overline{\phi}(\boldsymbol{G}(s)) + \overline{\phi}(\boldsymbol{H}(s)) \right] < \pi , \tag{35}$$

$$\inf_{s \in j[0,\infty]\setminus j\Omega} \left[ \underline{\phi}(\boldsymbol{G}(s)) + \underline{\phi}(\boldsymbol{H}(s)) \right] > -\pi . \tag{36}$$

*Proof:* See [23]. □

If the system $\boldsymbol{G}\#\boldsymbol{H}$ has a block structure, e.g., a networked distributed power system, we can show the following:

*Proposition 3 (Generalized Small Phase Theorem with Block Structure):* Consider the system $\boldsymbol{G}\#\boldsymbol{H}$ with the block structure $\boldsymbol{H} = \bigoplus_n \boldsymbol{T}_n(s)$ and $\boldsymbol{G} = \boldsymbol{B}^\dagger \bigoplus_e \boldsymbol{\mathcal{T}}_e(s)\boldsymbol{B}$ for some $\boldsymbol{B}$ of appropriate dimensions. For each $n$, let $\boldsymbol{T}_n(s) \in \mathcal{RH}_\infty$ be frequency-wise sectorial. For each $e$, let $\boldsymbol{\mathcal{T}}_e(s)$ be semi-stable frequency-wise semi-sectorial individually and along the indented imaginary axis, avoiding the poles of all $\boldsymbol{\mathcal{T}}_e(s)$ for indents smaller than some finite $\epsilon^*$. Write $j\Omega$ for the union of the set of poles on the imaginary axis. Assume that $\boldsymbol{G}(s)$ has constant rank along the contour. Then, the interconnected system $\boldsymbol{G}\#\boldsymbol{H}$ is stable if

$$\max_n \overline{\phi}\left(\boldsymbol{T}_n(s)\right) - \min_n \underline{\phi}\left(\boldsymbol{T}_n(s)\right) < \pi\,, \tag{37}$$

for all $s \in j[0,\infty]$, and

$$\max_e \overline{\phi}\left(\boldsymbol{\mathcal{T}}_e(s)\right) - \min_e \underline{\phi}\left(\boldsymbol{\mathcal{T}}_e(s)\right) \leq \pi\,, \tag{38}$$

for all $s \notin j\Omega$, and

$$\sup_{n,e,s\notin j\Omega} \left[\overline{\phi}\left(\boldsymbol{T}_n(s)\right) + \overline{\phi}\left(\boldsymbol{\mathcal{T}}_e(s)\right)\right] < \pi\,, \tag{39}$$

$$\inf_{n,e,s\notin j\Omega} \left[\underline{\phi}\left(\boldsymbol{T}_n(s)\right) + \underline{\phi}\left(\boldsymbol{\mathcal{T}}_e(s)\right)\right] > -\pi\,. \tag{40}$$

*Remark:* $\boldsymbol{H}$ is stable, and its sectoriality is ensured by (37). $\boldsymbol{G}$ is semi-stable, and its semi-sectoriality is ensured by (38) and the rank condition. Equations (39)–(40) imply the stability condition of Theorem 2.

*Proof:* We provide the proof in Appendix E. □

## Appendix C
## Linear Form of Power Grids With $V$ and $q$ Droop

To make use of Proposition 3, we have to linearize the power grid model under investigation into an appropriate form. In this section, we show that the power grid can be represented as an interconnected feedback system of two transfer matrices: $\boldsymbol{\mathcal{T}}^{\text{nod}}\#\boldsymbol{\mathcal{T}}^{\text{net}}$. $\boldsymbol{\mathcal{T}}^{\text{nod}}$ includes all nodal transfer matrices from $\hat{q}_n$ and $p_n$ to $\varrho_n$ and $\omega_n$, as in (3). $\boldsymbol{\mathcal{T}}^{\text{net}}$ represents the network structure and the physics of the coupling, as it takes $\boldsymbol{\varrho}$ and $\boldsymbol{\omega}$ as inputs and provides $\hat{\boldsymbol{q}}$ and $\boldsymbol{p}$ as outputs. The fundamental assumption we make is that the nodes can be modeled as voltage sources that react to conditions in the grid. This assumption is most natural in the context of grid-forming actors, such as power plants or grid-forming inverters.

### A. Complex Frequency Notation

As noted above, every node has a complex voltage (representing a balanced three-phase voltage) $v_n = v_{d,n} + jv_{q,n}$:

$$v_n(t) = V_n(t)e^{j\varphi_n(t)} = e^{\theta_n(t)}\,, \tag{41}$$

and a complex current $\imath_n$. The latter is given in terms of the former through the admittance matrix $\boldsymbol{Y}$:

$$\boldsymbol{\imath}(t) = \boldsymbol{Y}\cdot\boldsymbol{v}(t) = -j\boldsymbol{L}\cdot\boldsymbol{v}(t)\,. \tag{42}$$

The matrix $\boldsymbol{L} := je^{-j\kappa}\boldsymbol{Y} \in \mathbb{R}^{N\times N}$ is a real, symmetric, positive definite Laplacian. We show the proof for lossless grids, where $\kappa = 0$. The lossy case goes analogously with a rotation, see Section V.

We use a power-invariant transformation from $ABC$ coordinates, so that the apparent power is given by $S_n(t) = v_n(t)\overline{\imath}_n(t) = p_n(t) + jq_n(t)$ with active power $p_n(t)$ and reactive power $q_n(t)$.

Milano [19] suggests writing the nodal dynamics through the time derivative of the complex phase $\theta_n$, the complex frequency $\eta$:

$$\eta_n(t) = \dot{\theta}_n(t)\,, \tag{43}$$

$$\dot{v}_n(t) = \eta_n(t)v_n(t) \tag{44}$$

$$= (\varrho_n(t) + j\omega_n(t))v_n(t)\,. \tag{45}$$

We will drop the explicit time dependence $(t)$ from now on. By considering both, the complex equation and the complex conjugate equation,

$$\dot{v}_n = \eta_n v_n\,, \tag{46}$$

$$\dot{\overline{v}}_n = \overline{\eta}_n \overline{v}_n\,, \tag{47}$$

we can switch back and forth between complex and real picture, using a linear transformation. The velocities $\varrho_n$, $\omega_n$, $\eta_n$ and $\overline{\eta}_n$ are related by:

$$\begin{bmatrix}\eta_n\\ \overline{\eta}_n\end{bmatrix} = \begin{bmatrix}1 & j\\ 1 & -j\end{bmatrix}\begin{bmatrix}\varrho_n\\ \omega_n\end{bmatrix} = \boldsymbol{U}\begin{bmatrix}\varrho_n\\ \omega_n\end{bmatrix}\,, \tag{48}$$

$$\begin{bmatrix}\varrho_n\\ \omega_n\end{bmatrix} = \frac{1}{2}\begin{bmatrix}1 & 1\\ -j & j\end{bmatrix}\begin{bmatrix}\eta_n\\ \overline{\eta}_n\end{bmatrix} = \frac{1}{2}\boldsymbol{U}^\dagger\begin{bmatrix}\eta_n\\ \overline{\eta}_n\end{bmatrix}\,, \tag{49}$$

Note that $\boldsymbol{U}^{-1} = \frac{1}{2}\boldsymbol{U}^\dagger$, thus $\boldsymbol{U}/\sqrt{2}$ is a unitary matrix. This means that under $\boldsymbol{U}$ as coordinate transformation, all pertinent properties of linear dynamical systems are retained.

### B. A System of Grid-Forming Actors

We are interested in conditions that guarantee small-signal stability of a heterogeneous system of grid-forming actors, without strong assumptions on their internal structure. As noted above, we assume that we can model the nodes as voltages reacting to the grid state. We assume that the voltages react in a smooth, differentiable manner, and that $V_n > 0$. Thus, $\omega_n$ and $\varrho_n$ are defined, and can be chosen as the nodal output variable. Using $p_n$ and $q_n$ as the input that the nodal actor sees from the grid, we can write the general form of a node's behavior in terms of three functions $r_n$, $o_n$ and $\boldsymbol{f}_n^{\boldsymbol{x}}$:

$$\varrho_n = r_n(\varphi_n, V_n, p_n, q_n, \boldsymbol{x}_n)\,, \tag{50}$$

$$\omega_n = o_n(\varphi_n, V_n, p_n, q_n, \boldsymbol{x}_n)\,, \tag{51}$$

$$\dot{\boldsymbol{x}}_n = \boldsymbol{f}_n^{\boldsymbol{x}}(\varphi_n, V_n, p_n, q_n, \boldsymbol{x}_n)\,. \tag{52}$$

Here, $\boldsymbol{x}_n \in \mathbb{R}^{n_{\text{var}}}$ are internal states of dimension $n_{\text{var}}$ that reflect the inner workings of the grid actor, and are not visible directly in the output $v$. Examples include generator frequencies, inner-loop DC voltages, or the $d$- and $q$-components of internal AC quantities.

We make two assumptions on the form of the functions $r_n$, $o_n$ and $\boldsymbol{f}_n^{\boldsymbol{x}}$: I) Following [20], we assume that the nodal dynamics does not explicitly depend on $\varphi_n$. This assumption is justified by symmetry considerations and the desire not to introduce harmonic disturbances into the grid. II) We assume that the

reaction to a deviation in the voltage mirrors that of a deviation in the reactive power. That is, we assume that near the operation point, $r_n$, $o_n$, and $\boldsymbol{f}_n^{\boldsymbol{x}}$ only depend on $\hat{q}_n = q_n + \alpha_n V_n$ for some real $\alpha_n$ rather than on both $q_n$ and $V_n$ separately. With these assumptions, we have:

$$\varrho_n = r_n(p_n, \hat{q}_n, \boldsymbol{x}_n)\,, \tag{53}$$

$$\omega_n = o_n(p_n, \hat{q}_n, \boldsymbol{x}_n)\,, \tag{54}$$

$$\dot{\boldsymbol{x}}_n = \boldsymbol{f}_n^{\boldsymbol{x}}(p_n, \hat{q}_n, \boldsymbol{x}_n)\,. \tag{55}$$

### C. The Linearized Nodal Response

We define the coefficients of the Jacobian as

$$J_n^{\omega p} := \frac{\partial o_n}{\partial p_n}\,, \quad J_n^{\varrho\hat{q}} = \frac{\partial r_n}{\partial \hat{q}_n}\,, \quad \boldsymbol{J}_n^{xx} = \frac{\partial \boldsymbol{f}_n^{x}}{\partial \boldsymbol{x}_n}\,, \quad \text{etc.} \tag{56}$$

We now want to look at the linear response of the nodal subsystem around an operating point $v_n^\circ, i_n^\circ$. We assume that the operating point satisfies $\varrho_n^\circ = \omega_n^\circ = \dot{\boldsymbol{x}}_n = 0$. Write $\Delta p_n = p_n - p_n^\circ$ and $\Delta\hat{q}_n = q_n - q_n^\circ + \alpha_n(V_n - V_n^\circ)$ and assume that $\boldsymbol{x}_n^\circ = \boldsymbol{0}$. The linearized nodal dynamics are then

$$\dot{\boldsymbol{x}}_n = \boldsymbol{J}_n^{xp}\Delta p_n + \boldsymbol{J}_n^{xq}\Delta\hat{q}_n + \boldsymbol{J}_n^{xx}\boldsymbol{x}_n\,, \tag{57}$$

$$\varrho_n = J_n^{\varrho p}\Delta p_n + J_n^{\varrho\hat{q}}\Delta\hat{q}_n + \boldsymbol{J}_n^{\varrho x}\boldsymbol{x}_n\,, \tag{58}$$

$$\omega_n = J_n^{\omega p}\Delta p_n + J_n^{\omega\hat{q}}\Delta\hat{q}_n + \boldsymbol{J}_n^{\omega x}\boldsymbol{x}_n\,, \tag{59}$$

which we stack as

$$\dot{\boldsymbol{x}}_n = \boldsymbol{J}_n^{xqp}\begin{bmatrix}\Delta\hat{q}_n\\ \Delta p_n\end{bmatrix} + \boldsymbol{J}_n^{xx}\boldsymbol{x}_n\,, \tag{60}$$

$$\begin{bmatrix}\varrho_n\\ \omega_n\end{bmatrix} = \boldsymbol{J}_n^{\varrho\omega\hat{q}p}\begin{bmatrix}\Delta\hat{q}_n\\ \Delta p_n\end{bmatrix} + \boldsymbol{J}_n^{\varrho\omega x}\boldsymbol{x}_n\,. \tag{61}$$

The nodal transfer matrix from $[\Delta\hat{q}_n \quad \Delta p_n]^\intercal$ to $[\varrho_n \quad \omega_n]^\intercal$ is then just

$$-\boldsymbol{T}_n(s) = \boldsymbol{J}_n^{\varrho\omega\hat{q}p} + \boldsymbol{J}_n^{\varrho\omega x}(s - \boldsymbol{J}_n^{xx})^{-1}\boldsymbol{J}_n^{xqp}\,. \tag{62}$$

We can summarize the transfer matrices of all nodes in $\boldsymbol{T}^{\mathrm{nod}}$ such that

$$\begin{bmatrix}\boldsymbol{\varrho}\\ \boldsymbol{\omega}\end{bmatrix} = -\boldsymbol{T}^{\mathrm{nod}}\begin{bmatrix}\Delta\hat{\boldsymbol{q}}\\ \Delta\boldsymbol{p}\end{bmatrix} := -\bigoplus_n \boldsymbol{T}_n(s)\begin{bmatrix}\Delta\hat{\boldsymbol{q}}\\ \Delta\boldsymbol{p}\end{bmatrix}. \tag{63}$$

### D. The Linearized Network Response

To obtain the full linearized equations, we need the response of $\Delta p_n$ and $\Delta\hat{q}_n$ to variations in the complex angle $\theta_n$ around a given power flow with $\theta_n^\circ$.

This is most easily given in terms of a variant of the complex power and the complex couplings introduced by [21]. We define

$$\sigma_n := q_n + jp_n\,, \tag{64}$$

to mirror the definition of the complex frequency [19]. In terms of the usual complex power, this is $\sigma_n = j\overline{S}_n$. This complex power can be expressed in terms of the Hermitian matrix $\boldsymbol{K} \in \mathbb{C}^{N\times N}$ of complex couplings [19], [21]:

$$K_{nm} = \overline{v}_n L_{nm} v_m\,, \tag{65}$$

$$\sigma_n = \sum_m K_{nm}\,. \tag{66}$$

These quantities have a very simple derivative with respect to the complex phases of the system:

$$\frac{\partial K_{nm}}{\partial\theta_h} = \delta_{hm}K_{nm}\,, \qquad \frac{\partial K_{nm}}{\partial\overline{\theta}_h} = \delta_{hn}K_{nm}\,, \tag{67}$$

$$\frac{\partial\sigma_n}{\partial\theta_h} = K_{nh}\,, \qquad \frac{\partial\sigma_n}{\partial\overline{\theta}_h} = \delta_{nh}\sigma_n\,. \tag{68}$$

The linearization of $\sigma_n$ around an operating state of the system with complex couplings $K_{nm}^\circ$ and complex power $\sigma_n^\circ$ is then given by

$$\sigma_n \approx \sigma_n^\circ + \sigma_n^\circ\Delta\overline{\theta}_n + \sum_m K_{nm}^\circ\Delta\theta_m \tag{69}$$

or, in vector notation,

$$\begin{bmatrix}\Delta\boldsymbol{\sigma}\\ \Delta\overline{\boldsymbol{\sigma}}\end{bmatrix} \approx \begin{bmatrix}\boldsymbol{K}^\circ & [\boldsymbol{\sigma}^\circ]\\ [\overline{\boldsymbol{\sigma}}^\circ] & \overline{\boldsymbol{K}}^\circ\end{bmatrix}\begin{bmatrix}\Delta\boldsymbol{\theta}\\ \Delta\overline{\boldsymbol{\theta}}\end{bmatrix}. \tag{70}$$

As the nodal dynamics depend on $\Delta\hat{q}_n$ and $\Delta p_n$, as inputs, we now consider

$$\Delta\sigma_n + \alpha_n\Delta V_n = \Delta\hat{q}_n + j\Delta p_n\,, \tag{71}$$

for the output of the edge dynamics. Together with $\Delta V_n \approx V_n^\circ\frac{1}{2}(\Delta\theta + \Delta\overline{\theta})$, we obtain

$$\begin{bmatrix}\Delta\boldsymbol{\sigma} + \boldsymbol{\alpha}\Delta\boldsymbol{V}\\ \Delta\overline{\boldsymbol{\sigma}} + \boldsymbol{\alpha}\Delta\boldsymbol{V}\end{bmatrix} \approx \boldsymbol{J}^{\mathrm{net}}\begin{bmatrix}\Delta\boldsymbol{\theta}\\ \Delta\overline{\boldsymbol{\theta}}\end{bmatrix}, \tag{72}$$

with the transfer matrix

$$\boldsymbol{J}^{\mathrm{net}} := \begin{bmatrix}\boldsymbol{K}^\circ + \frac{1}{2}[\boldsymbol{\alpha}][\boldsymbol{V}^\circ] & [\boldsymbol{\sigma}^\circ] + \frac{1}{2}[\boldsymbol{\alpha}][\boldsymbol{V}^\circ]\\ [\overline{\boldsymbol{\sigma}}^\circ] + \frac{1}{2}[\boldsymbol{\alpha}][\boldsymbol{V}^\circ] & \overline{\boldsymbol{K}}^\circ + \frac{1}{2}[\boldsymbol{\alpha}][\boldsymbol{V}^\circ]\end{bmatrix}. \tag{73}$$

Note that $\boldsymbol{K}^\circ$ is Hermitian, and so is $\boldsymbol{J}^{\mathrm{net}}$. Further, we see from (66) that $[\boldsymbol{1} \quad -\boldsymbol{1}]^\intercal$ is a zero mode of the network response $\boldsymbol{J}^{\mathrm{net}}$.

At this point, we can see the necessity of incorporating the $V$ and $q$ droop into the network response. Without the presence of the $\alpha_n$, $\boldsymbol{J}^{\mathrm{net}}$ would be indefinite and thus not amenable to sectorial analysis.

### E. The Full System

Above we derived the nodal transfer matrix from $p_n$, $q_n + \alpha_n V_n$ to $\varrho_n$ and $\omega_n$, and the network response from $\theta_n$ and $\overline{\theta}_n$ to $\sigma_n + \alpha_n V_n$ and $\overline{\sigma}_n + \alpha_n V_n$. We can now combine these into the full system equations. Recall that

$$\Delta\dot{\theta}_n = \eta_n\,, \tag{74}$$

$$s\Delta\theta_n = \eta_n\,, \tag{75}$$

where the latter equation is in Laplace space. Let us introduce $\tilde{\boldsymbol{U}} \in \mathbb{C}^{2N\times 2N}$,

$$\tilde{\boldsymbol{U}} = \bigoplus_n \boldsymbol{U}\,. \tag{76}$$

With this, we can write the network response from a deviation in $\varrho$ and $\omega$ to a deviation in $\hat{q}$ and $p$ as

$$\boldsymbol{\mathcal{T}}^{\mathrm{net}}(s) = \frac{1}{2}\tilde{\boldsymbol{U}}^\dagger\frac{1}{s}\boldsymbol{J}^{\mathrm{net}}\tilde{\boldsymbol{U}}\,. \tag{77}$$

The full system $\boldsymbol{T}^{\mathrm{nod}}\#\boldsymbol{\mathcal{T}}^{\mathrm{net}}$ then has the structure

$$\bigoplus_n \boldsymbol{T}_n(s) \,\#\, \boldsymbol{\mathcal{T}}^{\mathrm{net}}(s)\,. \tag{78}$$

The major remaining challenge to applying Proposition 3 and getting decentralized conditions is to decompose this matrix into edge-wise contributions. As we will see in the next section, we can treat the network response as a superposition of two-node systems.

## APPENDIX D
## PROOF OF THE MAIN PROPOSITION 1

We now proceed to the proof of the main proposition. The first step is to provide conditions for the sectoriality of the nodal transfer matrices. Then, we provide the edge-wise decomposition of the network response, and demonstrate under which conditions it is semi-stable frequency-wise semi-sectorial. The main Theorem then follows by applying Proposition 3.

### A. Sectoriality of the Nodal Transfer Matrix

Each $\boldsymbol{T}_n(s)$ of the form (3) is a complex $2\times 2$ matrix. Here, we give conditions that ensure that it is strictly accretive, meaning the numerical range is contained in the open right half plane: $\underline{\phi} > -\pi/2$ and $\overline{\phi} < \pi/2$. Is gives especially concise conditions for sectoriality.

*Lemma 4:* A complex $2\times 2$ matrix $\boldsymbol{T}_n(s)$ is strictly accretive, hence sectorial, if and only if its four entries [see (3)] fulfill (4) and (5):

$$\Re(T_n^{\omega p}) + \Re(T_n^{\varrho\hat{q}}) > 0\,, \tag{79}$$

$$\Re(T_n^{\omega p})\cdot\Re(T_n^{\varrho\hat{q}}) > \frac{1}{4}\left|T_n^{\omega\hat{q}} + \overline{T}_n^{\varrho p}\right|^2\,. \tag{80}$$

*Proof:* If the numerical range $W$ of $\boldsymbol{T}_n$ (see (33)) is contained in the right-hand side, the real part of $W(\boldsymbol{T}_n)$ has to be strictly positive: $\Re(W(\boldsymbol{T}_n(s))) > 0$. The real part of the numerical range is given by the numerical range of the Hermitian part of $\boldsymbol{T}_n(s)$, which we denote $\hat{\boldsymbol{T}}_n(s) = \frac{1}{2}(\boldsymbol{T}_n(s) + \boldsymbol{T}_n(s)^\dagger)$. The numerical range of a Hermitian matrix is on the real axis. It is strictly positive if and only if the matrix is positive definite. The two-by-two matrix $\hat{\boldsymbol{T}}_n(s)$ is positive definite if and only if its determinant and its trace are positive. Expressed in terms of the matrix elements of $\boldsymbol{T}_n(s)$, these conditions are (4) and (5). □

### B. Edge-Wise Decomposition and Analysis of the Network Response

We now return to the network response. Our goal is to show that under the condition that [see (6)]

$$\alpha_n \geq \alpha_n^{\text{theory}} := 2\sum_m \tilde{Y}_{nm}\frac{V_m^\circ}{\cos(\varphi_n^\circ - \varphi_m^\circ)}, \tag{81}$$

we can decompose the network response into frequency-wise semi-stable and semi-sectorial edge contributions.

*Lemma 5:* $\boldsymbol{J}^{\text{net}}$ can be decomposed into edge-wise contributions $\boldsymbol{J}_e$ such that

$$\boldsymbol{J}^{\text{net}} = \boldsymbol{B}_+{}^\dagger \bigoplus_e \boldsymbol{J}_e \boldsymbol{B}_+\,, \tag{82}$$

if we introduce an edge-wise decomposition $\alpha'_{nm}$ of $\alpha_n$ such that

$$\alpha_n = -2V_n^\circ \sum_{m\neq n} L_{nm}\alpha'_{nm}. \tag{83}$$

*Proof:* The fundamental strategy is to collect the terms that represent each edge. In each of the four blocks of $\boldsymbol{J}^{\text{net}}$, the off-diagonal matrix elements naturally have an edge associated with them. The diagonal elements of $\boldsymbol{K}^\circ$ can be written as a sum of edge-wise contributions $K_{nn}^\circ = -|V_n^\circ|^2\sum_{m\neq n} L_{nm}$. The $\boldsymbol{\sigma}^\circ$ can be written as $\sigma_n^\circ = \sum_{m\neq n} K_{nm}^\circ - |V_n^\circ|^2\sum_{m\neq n} L_{nm}$. We then introduce a similar decomposition for $\frac{1}{2}\boldsymbol{\alpha}$ times $\boldsymbol{V}^\circ$, writing $\frac{1}{2}\alpha_n V_n^\circ = -|V_n^\circ|^2\sum_{m\neq n} L_{nm}\alpha'_{nm}$. Now, the contributions to the matrix elements of $\boldsymbol{J}^{\text{net}}$ associated to an edge $e=(n,m)$ all live on the rows and columns associated to $n$ and $m$. Thus, we can place them in a $4\times 4$ matrix $\boldsymbol{J}_e$ using the matrices $\boldsymbol{P}_e$ of (30) that pick out exactly those rows and columns.

To collect these edge-wise contributions, we introduce $C'_{nm} := \frac{\overline{v}_n^\circ}{v_n^\circ}(1+\alpha'_{nm}) - \frac{\overline{v}_m^\circ}{v_n^\circ}$. Then we can succinctly write the four-by-four matrix of elements originating from a single edge as $\boldsymbol{J}_e = -L_{nm}\boldsymbol{R}^\dagger\tilde{\boldsymbol{J}}_e\boldsymbol{R}$ with

$$\tilde{\boldsymbol{J}}_e = \begin{bmatrix} 1+\alpha'_{nm} & C'_{nm} & -1 & 0 \\ \overline{C}'_{nm} & 1+\alpha'_{nm} & 0 & -1 \\ -1 & 0 & 1+\alpha'_{mn} & C'_{mn} \\ 0 & -1 & \overline{C}'_{mn} & 1+\alpha'_{mn} \end{bmatrix} \tag{84}$$

and $\boldsymbol{R} := \operatorname{diag}(\overline{v}_n^\circ, v_n^\circ, \overline{v}_m^\circ, v_m^\circ)$. With this, (82) can be verified by straightforward calculation, collecting all terms associated to each edge. □

As $\boldsymbol{J}^{\text{net}}$, and the $\boldsymbol{J}_e$, are Hermitian, their numerical range is on the real axis. They are (semi-)sectorial if and only if they are (semi-)definite. In the phase stability theorems, it is assumed that the transfer matrix $G(\epsilon^+)$ has phase center zero. From (77) we see that this implies that $\boldsymbol{J}^{\text{net}}$ and thus $\boldsymbol{J}_e$ have to be positive semi-definite.

*Lemma 6:* $\boldsymbol{J}_e$ is positive semi-definite, hence semi-sectorial, if

$$|\varphi_n^\circ - \varphi_m^\circ| < \frac{\pi}{2} \quad \forall\, e=(n,m)\in\mathcal{E}, \tag{85}$$

$$\alpha'_{nm} \geq \frac{V_m^\circ}{V_n^\circ\cos(\varphi_n^\circ - \varphi_m^\circ)} - 1\,. \tag{86}$$

*Proof:* This can be verified with a straightforward calculation, e.g., using the Schur complement lemma. □

The edge-wise decomposition of $\alpha_n$ leaves us with the freedom to weight the $\alpha'_{nm}$ freely, as long as they satisfy (83). The tightest bound is achieved by weighting them proportional to the bounds derived in (86). However, we can achieve a much more concise node-wise condition for the $\alpha_n$, which are actual dynamical parameters of the nodal actors:

*Lemma 7:* $\boldsymbol{\mathcal{T}}^{\text{net}}(s)$ can be decomposed into semi-stable frequency-wise sectorial $\boldsymbol{\mathcal{T}}_e$ as

$$\boldsymbol{\mathcal{T}}^{\text{net}}(s) = \tilde{\boldsymbol{U}}^\dagger \boldsymbol{B}_+^\dagger \bigoplus_e \boldsymbol{\mathcal{T}}_e(s)\boldsymbol{B}_+\tilde{\boldsymbol{U}}\,, \tag{87}$$

if $\alpha_n \geq \alpha_n^{\text{theory}}$, i.e., (6) holds.

*Proof:* The $\boldsymbol{\mathcal{T}}_e(s)$ are given by

$$\boldsymbol{\mathcal{T}}_e := \frac{1}{2s}\boldsymbol{J}_e\,. \tag{88}$$

According to Lemma 6, (85) and (86) imply frequency-wise semi-sectorial $\boldsymbol{J}_e$ and thus $\boldsymbol{\mathcal{T}}_e$. The factor $1/s$ makes them semi-stable, because the pole is at zero and the rank is left constant along the contour. Using the definition of $\alpha'_{nm}$, we see that (86) can always be satisfied if $\alpha_n \geq \alpha_n^{\text{theory}}$. □

As $\bigoplus_e \boldsymbol{\mathcal{T}}_e(s)$ only depends on $s$ through scaling by a common factor, we also immediately have that its rank is constant along the contour. Thus, $\boldsymbol{\mathcal{T}}^{\text{net}}(s)$ is semi-stable frequency-wise semi-sectorial. On $s \in j(\epsilon^+, \infty]$ the phases of the $\boldsymbol{\mathcal{T}}_e(s)$ are simply: $\underline{\phi}(\boldsymbol{\mathcal{T}}_e) = -\frac{\pi}{2} = \overline{\phi}(\boldsymbol{\mathcal{T}}_e)$. on the quarter circle of radius $\epsilon^+$ from $j\epsilon^+$ to $\epsilon^+$, they rotate to 0.

In conclusion, (6) ensures semi-stable frequency-wise sectorial $\boldsymbol{\mathcal{T}}^{\text{net}}(s)$ with a DC phase center of 0, which is a pole, and all phases $-\frac{\pi}{2}$ at $s \in j\mathbb{R} \setminus j\Omega$.

### C. Putting Everything Together

*Proof:* We can now apply Proposition 3 to the system given by (78), with $\boldsymbol{H} = \boldsymbol{T}^{\text{nod}} = \bigoplus_n \boldsymbol{T}_n(s)$, $\boldsymbol{B} = \boldsymbol{B}_+\tilde{\boldsymbol{U}}$, and $\boldsymbol{G} = \boldsymbol{\mathcal{T}}^{\text{net}} = \boldsymbol{B}^\dagger \bigoplus_e \boldsymbol{\mathcal{T}}_e(s)\boldsymbol{B}$. We have shown in the previous sections that with (4)–(6), (i) the $\boldsymbol{T}_n$ in (3) and (62) are in $\mathcal{RH}_\infty$ (hence stable) and frequency-wise sectorial according to Lemma 4; (ii) the $\boldsymbol{\mathcal{T}}_e$ in (88) are semi-stable frequency-wise semi-sectorial according to Lemma 6. They are also semi-stable along the shared indented imaginary axis because they share the same poles. Finally, $\boldsymbol{G}$ has constant rank along the contour, because it depends on $s$ only by a prefactor $1/s$.

We now proceed to show that (37)–(40) hold. (37) is fulfilled for (4)–(5), as $\underline{\phi}(\boldsymbol{T}_n) > -\pi/2$ and $\overline{\phi}(\boldsymbol{T}_n) < \pi/2$. (38) is fulfilled, as $\underline{\phi}(\boldsymbol{\mathcal{T}}_e) = -\frac{\pi}{2} = \overline{\phi}(\boldsymbol{\mathcal{T}}_e)$. Similarly, the combined phases of $\boldsymbol{\mathcal{T}}^{\text{net}}$ and $\boldsymbol{T}^{\text{nod}}$ lie within $(-\pi, 0)$ at all $s \in j\mathbb{R} \setminus j\Omega$, hence (39) and (40) hold. This concludes the proof. □

As $\boldsymbol{\mathcal{T}}_e$ have phase $-\frac{\pi}{2}$ at all non-zero frequencies, the phases of $\boldsymbol{T}_n$ need not be contained in the open right half plane. However, $\hat{\boldsymbol{T}}_n > 0$ is sufficient for our examples below and gives the most concise conditions.

## Appendix E
## Proof of Proposition 3

### A. Preliminaries

Let us recall two properties of $W'$ that will prove useful later on. First, it follows from the definition of $W'$ that

$$W'(\boldsymbol{B}^\dagger \boldsymbol{M} \boldsymbol{B}) \subseteq (W'(\boldsymbol{M}) \cup 0)\ , \tag{89}$$

for any $\boldsymbol{M} \in \mathbb{C}^{m\times m}$ and $\boldsymbol{B}$ of appropriate size, and therefore,

$$\overline{\phi}(\boldsymbol{B}^\dagger \boldsymbol{M} \boldsymbol{B}) \leq \overline{\phi}(\boldsymbol{M})\,, \qquad \underline{\phi}(\boldsymbol{B}^\dagger \boldsymbol{M} \boldsymbol{B}) \geq \underline{\phi}(\boldsymbol{M})\,. \tag{90}$$

Second, for a block diagonal system $\boldsymbol{M} = \bigoplus_e \boldsymbol{M}_e$, the numerical range is the convex hull of the blocks' numerical ranges [37, Property 1.2.10]:

$$W(\boldsymbol{M}) = \text{Conv}\left(W(\boldsymbol{M}_1), \ldots, W(\boldsymbol{M}_E)\right)\ . \tag{91}$$

Thus, if $\boldsymbol{M}$ is semi-sectorial,

$$\overline{\phi}(\boldsymbol{M}) = \max_e \overline{\phi}(\boldsymbol{M}_e)\,, \qquad \underline{\phi}(\boldsymbol{M}) = \min_e \underline{\phi}(\boldsymbol{M}_e)\,. \tag{92}$$

With this toolbox, we are now ready to prove our main result. The proof of Proposition 3 relies on the four following Lemmas.

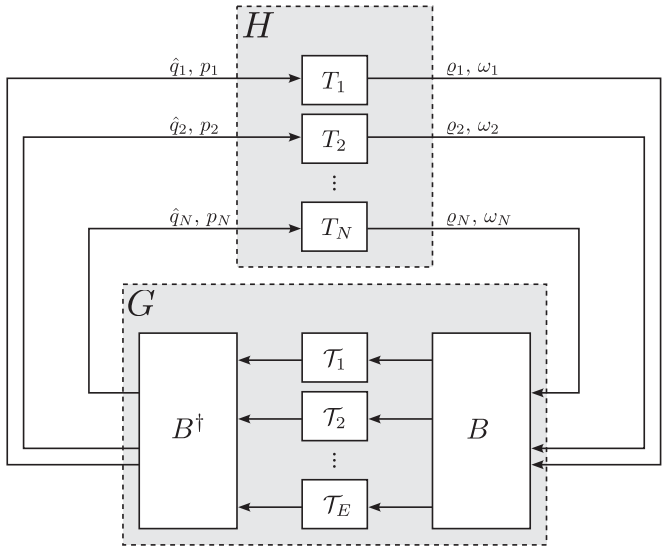


Fig. 4. Block diagram representation of the system considered. Block $H$ is the nodal response to the lines' output, and block $G$ is the lines' response to the nodes' dynamics.

*Lemma 8:* Let $\boldsymbol{T}_1, \ldots, \boldsymbol{T}_N$ be stable transfer matrices. Then $\boldsymbol{T}(s) = \bigoplus_n \boldsymbol{T}_n(s)$ is stable.

*Proof:* The transfer matrix $\boldsymbol{T}(s)$ is stable, because the set of its poles is the union of the poles of its blocks. □

*Lemma 9:* Let $\boldsymbol{T}_1, \ldots, \boldsymbol{T}_N$ be frequency-wise sectorial transfer matrices. Then, $\boldsymbol{T}(s) = \bigoplus_n T_n(s)$ is frequency-wise sectorial if and only if

$$\max_n \overline{\phi}\left(\boldsymbol{T}_n(s)\right) - \min_n \underline{\phi}\left(\boldsymbol{T}_n(s)\right) < \pi\,, \tag{93}$$

for all $s \in j[0, \infty]$, cf. (37).

*Proof:* Due to (91), we have that $W(\boldsymbol{T})$ is the convex hull of all $W(\boldsymbol{T}_n)$. Therefore, if (93) is satisfied for all, $W(\boldsymbol{T})$ is contained in a sector of angle $\delta(\boldsymbol{T}) < \pi$. Furthermore, as none of the $W(\boldsymbol{T}_n)$ contain the origin, $W(\boldsymbol{T})$ does not contain the origin. We conclude that $\boldsymbol{T}$ is frequency-wise sectorial. Similarly, if $\boldsymbol{T}$ is frequency-wise sectorial, then none of the $W(\boldsymbol{T}_n)$ contains the origin, and they all lie in a sector of angle smaller than $\pi$, and (93) holds. All of the above holds for any $s \in j[0, \infty]$, which concludes the proof. □

*Lemma 10:* Let $\boldsymbol{\mathcal{T}}_1, \ldots, \boldsymbol{\mathcal{T}}_E$ be semi-stable transfer matrices and let us define $\boldsymbol{\mathcal{T}}(s) = \bigoplus_e \boldsymbol{\mathcal{T}}_e(s)$. Let $\boldsymbol{B}$ be a complex matrix of appropriate dimensions. Then both $\boldsymbol{\mathcal{T}}(s)$ and $\boldsymbol{B}^\dagger \boldsymbol{\mathcal{T}}(s)\boldsymbol{B}$ are semi-stable.

*Proof:* The transfer matrix $\boldsymbol{\mathcal{T}}(s)$ is semi-stable, because the set of its poles is the union of the poles of its blocks. As the matrix $\boldsymbol{B}$ cannot introduce new poles, the poles of $\boldsymbol{B}^\dagger \boldsymbol{\mathcal{T}}(s)\boldsymbol{B}$ form a subset of the poles of $\boldsymbol{T}(s)$. Therefore, $\boldsymbol{B}^\dagger \boldsymbol{\mathcal{T}}(s)\boldsymbol{B}$ is semi-stable. □

*Lemma 11:* Let $\boldsymbol{\mathcal{T}}_1, \ldots, \boldsymbol{\mathcal{T}}_E$ be frequency-wise semi-sectorial transfer matrices and let us define $\boldsymbol{T}(s) = \bigoplus_e \boldsymbol{\mathcal{T}}_e(s)$. Assume further that

$$\max_e \overline{\phi}\left(\boldsymbol{\mathcal{T}}_e(s)\right) - \min_e \underline{\phi}\left(\boldsymbol{\mathcal{T}}_e(s)\right) \leq \pi\,, \tag{94}$$

for all $s \in j\mathbb{R} \setminus j\Omega$, where $j\Omega$ is the union of the poles of $\boldsymbol{\mathcal{T}}_1, \ldots, \boldsymbol{\mathcal{T}}_E$ that lie on the imaginary axis, cf. (38). Assume that

$\boldsymbol{\mathcal{T}}_1, \ldots, \boldsymbol{\mathcal{T}}_E$ are all frequency-wise semi-sectorial, and assume furthermore that they are semi-sectorial along the indented imaginary axis, avoiding the poles of all $\boldsymbol{\mathcal{T}}_e(s)$ for indents smaller than some finite $\epsilon^*$. Finally, assume that $\boldsymbol{B}^\dagger \boldsymbol{\mathcal{T}}(s)\boldsymbol{B}$ has constant rank along this indented imaginary axis for some constant complex matrix $\boldsymbol{B}$ of appropriate dimensions. Then $\boldsymbol{B}^\dagger \boldsymbol{\mathcal{T}}(s)\boldsymbol{B}$ is frequency-wise semi-sectorial.

*Remark:* $\boldsymbol{\mathcal{T}(s)}$ is covered with $\boldsymbol{B} = \boldsymbol{I}$.

*Proof:* First, observe that if a meromorphic $\boldsymbol{\mathcal{T}}_e(s)$ has constant rank $r$ on a contour, it has constant rank on any infinitesimal deformation of the contour. A matrix of rank $r$ has a minor of order $r$ with non-zero determinant, and the determinants of all minors of order larger than $r$ are zero. As the minors are meromorphic functions, they are either identically zero or their zeros are isolated points. Thus, the rank can only change at isolated points of the meromorphic function. As the rank is constant on the contour, none of these points can be on the contour, and we can deform the contour, avoiding these points.

Take an $\epsilon < \epsilon^*$ such that for all $\epsilon' \leq \epsilon$, the imaginary axis with $\epsilon'$ indentation at $j\Omega$ does not hit a rank changing point of any $\boldsymbol{\mathcal{T}}_e(s)$, $e \in \{1, \ldots, E\}$.

By assumption, for all $e \in \{1, \ldots, E\}$, $\boldsymbol{\mathcal{T}}_e(s)$ is semi-sectorial and has constant rank on this $\epsilon$-indented imaginary axis (contour).

Combining (89), (91), and (94), semi-sectoriality of $\boldsymbol{\mathcal{T}}_1(s), \ldots, \boldsymbol{\mathcal{T}}_E(s)$ implies semi-sectoriality of $\boldsymbol{B}^\dagger \boldsymbol{\mathcal{T}}(s)\boldsymbol{B}$, for $s \in j\mathbb{R}$.

Furthermore, by assumption, $\boldsymbol{B}^\dagger \boldsymbol{\mathcal{T}}(s)\boldsymbol{B}$ has constant rank along the $\epsilon$-indented imaginary axis.

Altogether, the above implies that $\boldsymbol{B}^\dagger \boldsymbol{\mathcal{T}}(s)\boldsymbol{B}$ is frequency-wise semi-sectorial, which concludes the proof. □

### B. Proof of Proposition 3

*Proof:* By Lemma 8, $\boldsymbol{H} = \bigoplus_n \boldsymbol{T}_n$ is stable. By Lemma 9, $\boldsymbol{H}$ is frequency-wise sectorial if (37) holds. By Lemma 10, $\boldsymbol{G} = \boldsymbol{B}^\dagger \bigoplus_e \boldsymbol{\mathcal{T}}_e \boldsymbol{B}$ is semi-stable. By Lemma 11, $\boldsymbol{G}$ is frequency-wise semi-sectorial if (38) and the constant rank condition hold.

Using one more time the convex hull property (91), in particular (92), and the subset property (89), the assumptions (39)–(40) yield

$$\sup_{s \notin j\Omega} \left[ \overline{\phi} \left( \bigoplus_n \boldsymbol{T}_n \right) + \overline{\phi} \left( \boldsymbol{B}^\dagger \bigoplus_e \boldsymbol{\mathcal{T}}_e \boldsymbol{B} \right) \right] < \pi \,, \tag{95}$$

$$\inf_{s \notin j\Omega} \left[ \underline{\phi} \left( \bigoplus_n \boldsymbol{T}_n \right) + \underline{\phi} \left( \boldsymbol{B}^\dagger \bigoplus_e \boldsymbol{\mathcal{T}}_e \boldsymbol{B} \right) \right] > -\pi \,, \tag{96}$$

where $\boldsymbol{T}_n$ and $\boldsymbol{\mathcal{T}}_e$ are functions of $s$. These are the phase conditions (35)–(36) of Theorem 2. All in all, the system $(\bigoplus_n \boldsymbol{T}_n) \# (\boldsymbol{B}^\dagger \bigoplus_e \boldsymbol{\mathcal{T}}_e \boldsymbol{B})$ then satisfies all assumptions and conditions of Theorem 2 and is therefore stable, which concludes the proof. □

## REFERENCES


[1] A. Bergen and D. Hill, "A structure preserving model for power system stability analysis," *IEEE Trans. Power App. Syst.*, vol. PAS-100, no. 1, pp. 25–35, Jan. 1981.

[2] J. Machowski, J. Bialek, and J. Bumby, *Power System Dynamics. Stability and Control*. Hoboken, NJ, USA, Wiley, Jan. 2012.

[3] F. Dörfler, M. Chertkov, and F. Bullo, "Synchronization in complex oscillator networks and smart grids," in *Proc. Nat. Acad. Sci.*, Feb. 2013, vol. 110, no. 6, pp. 2005–2010. [Online]. Available: https://www.pnas.org/doi/full/10.1073/pnas.1212134110

[4] P. Yang, F. Liu, Z. Wang, and C. Shen, "Distributed stability conditions for power systems with heterogeneous nonlinear bus dynamics," *IEEE Trans. Power Syst.*, vol. 35, no. 3, pp. 2313–2324, May 2020. [Online]. Available: https://ieeexplore.ieee.org/abstract/document/8890862

[5] J. Schiffer, R. Ortega, A. Astolfi, J. Raisch, and T. Sezi, "Conditions for stability of droop-controlled inverter-based microgrids," *Automatica*, vol. 50, no. 10, pp. 2457–2469, Oct. 2014. [Online]. Available: https://www.sciencedirect.com/science/article/pii/S0005109814003100

[6] D. Witthaut, F. Hellmann, J. Kurths, S. Kettemann, H. Meyer-Ortmanns, and M. Timme, "Collective nonlinear dynamics and self-organization in decentralized power grids," *Rev. Modern Phys.*, vol. 94, no. 1, Feb. 2022, Art. no. 015005. [Online]. Available: https://link.aps.org/doi/10.1103/RevModPhys.94.015005

[7] P. C. Böttcher, L. R. Gorjão, and D. Witthaut, "Stability bounds of droop-controlled inverters in power grid networks," *IEEE Access*, vol. 11, pp. 119947–119958, 2023. [Online]. Available: https://ieeexplore.ieee.org/document/10267988/?arnumber=10267988

[8] L. Woolcock and R. Schmid, "Mixed gain/phase robustness criterion for structured perturbations with an application to power system stability," *IEEE Control Syst. Lett.*, vol. 7, pp. 3193–3198, 2023. [Online]. Available: https://ieeexplore.ieee.org/document/10167642/authors#authors

[9] R. Pates and G. Vinnicombe, "Scalable design of heterogeneous networks," *IEEE Trans. Autom. Control*, vol. 62, no. 5, pp. 2318–2333, May 2017. [Online]. Available: https://ieeexplore.ieee.org/document/7583731/?arnumber=7583731

[10] C. De Persis and N. Monshizadeh, "Bregman storage functions for microgrid control," *IEEE Trans. Autom. Control*, vol. 63, no. 1, pp. 53–68, Jan. 2018. [Online]. Available https://ieeexplore.ieee.org/document/7934382

[11] L. Huang et al., "Gain and phase: Decentralized stability conditions for power electronics-dominated power systems," *IEEE Trans. Power Syst.*, vol. 39, no. 6, pp. 7240–7256, Nov. 2024. [Online] Available: https://ieeexplore.ieee.org/document/10477540

[12] P. Christensen et al., "High penetration of power electronic interfaced power sources and the potential contribution of grid forming converters," Brussels, Jan. 2020. [Online]. Available: https://www.entsoe.eu/events/2020/01/30/workshop-on-high-penetration-of-power-electronic-interfaced-power-sources-and-the-potential-contribution-of-grid-forming-converters/

[13] A. Dyśko et al., "Testing characteristics of grid forming converters part III: Inertial behaviour," in *Proc. 19th Wind Integration Workshop*, 2020. [Online]. Available: https://scholar.google.de/citations?view_op=view_citation&hl=de&user=ZxSUL5IAAAAJ&pagesize=80&sortby=pubdate&citation_for_view=ZxSUL5IAAAAJ:_Ybze24A_UAC

[14] M. Chen, D. Zhou, A. Tayyebi, E. Prieto-Araujo, F. Dörfler, and F. Blaabjerg, "Generalized multivariable grid-forming control design for power converters," *IEEE Trans. Smart Grid*, vol. 13, no. 4, pp. 2873–2885, Jul. 2022. [Online]. Available: https://ieeexplore.ieee.org/document/9739797/?arnumber=9739797

[15] V. Häberle, A. Tayyebi, X. He, E. Prieto-Araujo, and F. Dörfler, "Grid-forming and spatially distributed control design of dynamic virtual power plants," *IEEE Trans. Smart Grid*, vol. 15, no. 2, pp. 1761–1777, Mar. 2024. [Online]. Available: https://ieeexplore.ieee.org/document/10239108

[16] X. He, L. Huang, I. Subotić, V. Häberle, and F. Dörfler, "Quantitative stability conditions for grid-forming converters with complex droop control," *IEEE Trans. Power Electron.*, vol. 39, no. 9, pp. 10834–10852, Sep. 2024. [Online]. Available: https://ieeexplore.ieee.org/document/10536651/

[17] J. Schiffer, D. Zonetti, R. Ortega, A. M. Stanković, T. Sezi, and J. Raisch, "A survey on modeling of microgrids—From fundamental physics to phasors and voltage sources," *Automatica*, vol. 74, pp. 135–150, Dec. 2016. [Online]. Available: https://www.sciencedirect.com/science/article/pii/S0005109816303041

[18] K. Schmietendorf, J. Peinke, R. Friedrich, and O. Kamps, "Self-organized synchronization and voltage stability in networks of synchronous machines," *Eur. Phys. J. Special Topics*, vol. 223, no. 12, pp. 2577–2592, Oct. 2014. [Online]. Available: https://doi.org/10.1140/epjst/e2014-02209-8

[19] F. Milano, "Complex frequency," *IEEE Trans. Power Syst.*, vol. 37, no. 2, pp. 1230–1240, Mar. 2022. [Online]. Available: https://ieeexplore.ieee.org/document/9524491

[20] R. Kogler, A. Plietzsch, P. Schultz, and F. Hellmann, "Normal form for grid forming power grid actors," PRX Energy 1, 013008 – Jun. 30, 2022, *doi: 10.1103/PRXEnergy.1.013008*.
[21] A. Büttner and F. Hellmann, "Complex couplings–a universal, adaptive and bilinear formulation of power grid dynamics," *PRX Energy*, vol. 3, no. 1, Feb. 2024, Art. no. 013005.
[22] A. Büttner, H. Würfel, S. Liemann, J. Schiffer, and F. Hellman, "Complex-phase, data-driven identification of grid-forming inverter dynamics," *IEEE Trans. Smart Grid*, early access, Jul., 23 2025, doi: 10.1109/TSG.2025.3591891.
[23] W. Chen, D. Wang, S. Z. Khong, and L. Qiu, "A phase theory of multi-input multi-output linear time-invariant systems," *SIAM J. Control Optim.*, vol. 62, no. 2, pp. 1235–1260, Apr. 2024. [Online]. Available: https://epubs.siam.org/doi/10.1137/22M148968X
[24] N. Kastendiek, J. Niehues, R. Delabays, T. Gross, and F. Hellmann, "Phase and gain stability for adaptive dynamical networks," *Chaos: Interdiscipl. J. Nonlinear Sci.*, vol. 35, no. 5, May 2025, Art. no. 053142. [Online]. Available: https://doi.org/10.1063/5.0249706
[25] R. Berner, T. Gross, C. Kuehn, J. Kurths, and S. Yanchuk, "Adaptive dynamical networks," 2023, *arXiv:2304.05652*.
[26] I. C. Lestas and G. Vinnicombe, "Scalable robust stability for nonsymmetric heterogeneous networks," *Automatica*, vol. 43, no. 4, pp. 714–723, Apr. 2007. [Online]. Available: https://www.sciencedirect.com/science/article/pii/S0005109806004523
[27] X. He and F. Dörfler, "Passivity and decentralized stability conditions for grid-forming converters," *IEEE Trans. Power Syst.*, vol. 39, no. 3, pp. 5447–5450, May 2024. [Online] Available: https://ieeexplore.ieee.org/document/10417814
[28] V. Häberle, X. He, L. Huang, F. Dörfler, and S. Low, "Decentralized parametric stability certificates for grid-forming converter control," 2025, *arXiv:2503.05403*.
[29] Z. Shuai, C. Shen, X. Liu, Z. Li, and Z. J. Shen, "Transient angle stability of virtual synchronous generators using Lyapunov's direct method," *IEEE Trans. Smart Grid*, vol. 10, no. 4, pp. 4648–4661, Jul. 2019. [Online]. Available: https://ieeexplore.ieee.org/document/8444083/?arnumber=8444083
[30] J. W. Simpson-Porco, F. Dörfler, and F. Bullo, "Voltage stabilization in microgrids via quadratic droop control," *IEEE Trans. Autom. Control*, vol. 62, no. 3, pp. 1239–1253, Mar. 2017, [Online]. Available: https://ieeexplore.ieee.org/abstract/document/7500071
[31] J. Fritzsch and P. Jacquod, "Stabilizing large-scale electric power grids with adaptive Inertia," *PRX Energy*, vol. 3, no. 3, Aug. 2024, Art. no. 033003. [Online]. Available: https://link.aps.org/doi/10.1103/PRXEnergy.3.033003
[32] P. C. Böttcher, D. Witthaut, and L. Rydin Gorjão, "Dynamic stability of electric power grids: Tracking the interplay of the network structure, transmission losses, and voltage dynamics," *Chaos: An Interdiscipl. J. Nonlinear Sci.*, vol. 32, no. 5, May 2022, Art. no. 053117. [Online]. Available: https://doi.org/10.1063/5.0082712
[33] V. Häberle, L. Huang, X. He, E. Prieto-Araujo, and F. Dörfler, "Dynamic ancillary services: From grid codes to transfer function-based converter control," *Elect. Power Syst. Res.*, vol. 234, 2024, Art. no. 110760, doi: 10.1016/j.epsr.2024.110760.
[34] D. Moutevelis, J. Roldán-Pérez, M. Prodanovic, and F. Milano, "Taxonomy of power converter control schemes based on the complex frequency concept," *IEEE Trans. Power Syst.*, vol. 39, no. 1, pp. 1996–2009, Jan. 2024. [Online]. Available: https://ieeexplore.ieee.org/abstract/document/10105508
[35] G.-S. Seo, M. Colombino, I. Subotic, B. Johnson, D. Groß, and F. Dörfler, "Dispatchable virtual oscillator control for decentralized inverter-dominated power systems: Analysis and experiments," in *Proc. IEEE Appl. Power Electron. Conf. Expo.*, Mar. 2019, pp. 561–566.
[36] D. Groß, M. Colombino, J.-S. Brouillon, and F. Dörfler, "The effect of transmission-line dynamics on grid-forming dispatchable virtual oscillator control," *IEEE Trans. Control Netw. Syst.*, vol. 6, no. 3, pp. 1148–1160, Sep. 2019.
[37] R. A. Horn and C. R. Johnson, *Top. in Matrix Anal.*, 1st ed. Cambridge, U.K.: Cambridge Univ. Press, Apr. 1991. [Online]. Available: https://www.cambridge.org/core/product/identifier/9780511840371/type/book
[38] D. Wang, W. Chen, S. Z. Khong, and L. Qiu, "On the phases of a complex matrix," *Linear Algebra its Appl.*, vol. 593, pp. 152–179, May 2020. [Online]. Available: https://www.sciencedirect.com/science/article/pii/S0024379520300458
[39] D. Wang, X. Mao, W. Chen, and L. Qiu, "On the phases of a semi-sectorial matrix and the essential phase of a Laplacian," *Linear Algebra its Appl.*, vol. 676, pp. 441–458, Nov. 2023. [Online]. Available: https://www.sciencedirect.com/science/article/pii/S0024379523002744
[40] A. Büttner, F. Hellmann, and J. Niehues, "Small-signal stability of power systems with voltage droop," Oct. 2025, Art. no. 110760, doi: 10.5281/zenodo.17292389.

**Jakob Niehues** (Graduate Student Member, IEEE) is currently a Doctoral Researcher at Technische Universität Berlin, Germany and the Potsdam Institute for Climate Impact Research. He studied physics with Humboldt University of Berlin, Germany, and the Niels Bohr Institute, Copenhagen, Denmark. His research focuses on the dynamics and stability of complex networks, such as renewable power grids. He was the recipient of the Lise Meitner Award for his outstanding master's thesis. Since 2024, he has been a Fellow at the Berlin Mathematical School.

**Robin Delabays** received the Ph.D. degree from the University of Geneva, Switzerland, in 2018. He was a Postdoctoral Researcher at UC Santa Barbara. Since 2022, he is an Assistant Professor at the University of Applied Sciences of Western Switzerland (HES-SO), Sion, Switzerland. His research focuses on the intersection between dynamical systems and complex networks, with a special focus on the stability of power grids.

**Anna Büttner** (Member, IEEE) received the B.Sc. and M.Sc. degrees in physics in 2018 and 2021, respectively, after studying in Berlin, Germany, and Amsterdam, The Netherlands, and the Ph.D. degree in 2025 for her work on the dynamics and stability of future power grids. She is currently a Postdoctoral Researcher at the Potsdam Institute for Climate Impact Research, Potsdam, Germany. Her research interests include the application of dynamical systems theory to the energy transition.

**Frank Hellmann** (Member, IEEE) received the Ph.D. degree in theoretical physics from the University of Nottingham, U.K., in 2011. After initially working in Quantum Gravity, he switched to Complex Systems, with a focus on renewable power grids. Since 2018, he has been leading the Infrastructure and Complex Networks group at the Complexity Science Department of the Potsdam Institute for Climate Impact Research. His research focuses on new methods for modeling power grids, analytical and numerical stability properties of complex systems, and the interplay of extreme events and intrinsic behaviors of networks.